GUT MICROBES
2025, VOL. 17, NO. 1, 2488105
https://doi.org/10.1080/19490976.2025.2488105

Taylor & Francis
Taylor & Francis Group

RESEARCH PAPER

OPEN ACCESS Check for updates

Raffinose-metabolizing bacteria impair radiation-associated hematopoietic recovery *via* the bile acid/FXR/NF-κB signaling pathway

Yang Jiao[a,b,c*], Jiawei Ren[a,b*], Shichang Xie[d*], Nan Yuan[a,b], Jiaqi Shen[a,e,f,g], Huafang Yin[h], Jian Wang[h], Hongjuan Guo[a,b], Jianping Cao[a,b], Xin Wang[i], Depei Wu[a,c,e,f,g], Zhemin Zhou[d,j,k], and Xiaofei Qi[c,e,f]

[a]State Key Laboratory of Radiation Medicine and Protection, School of Radiation Medicine and Protection, Soochow University, Suzhou, China; [b]Collaborative Innovation Center of Radiological Medicine of Jiangsu Higher Education Institutions, Soochow University, Suzhou, China; [c]National Clinical Research Center for Hematologic Diseases, Jiangsu Institute of Hematology, Collaborative Innovation Center of Hematology, Suzhou, China; [d]Key Laboratory of Alkene-Carbon Fibers-Based Technology & Application for Detection of Major Infectious Diseases, MOE Key Laboratory of Geriatric Diseases and Immunology, Cancer Institute, Suzhou Medical College, Soochow University, Suzhou, China; [e]Department of Hematology, The First Affiliated Hospital of Soochow University, Suzhou, China; [f]Cyrus Tang Hematology Center, Soochow University, Suzhou, China; [g]Institute of Blood and Marrow Transplantation, Soochow University, Suzhou, China; [h]The Affiliated Jiangyin People's Hospital of Nantong University, Jiangyin, China; [i]State Key Laboratory for Managing Biotic and Chemical Threats to the Quality and Safety of Agro-Products & Institute of Food Sciences, Zhejiang Academy of Agricultural Sciences, Hangzhou, China; [j]Cancer Institute, Suzhou Medical College, The Second Affiliated Hospital of Soochow University, Suzhou, China; [k]National Center of Technology Innovation for Biopharmaceuticals, Suzhou Biomedical Industry Innovation Center, Suzhou, China

ABSTRACT

Radiation-associated hematopoietic recovery (RAHR) is critical for mitigating lethal complications of acute radiation syndrome (ARS), yet therapeutic strategies remain limited. Through integrated multi-omics analysis of a total body irradiation (TBI) mouse model, we identify *Bacteroides acidifaciens*-dominated gut microbiota as key mediators of RAHR impairment. 16S ribosomal rRNA sequencing revealed TBI-induced dysbiosis characterized by *Bacteroidaceae* enrichment, while functional metagenomics identified raffinose metabolism as the most significantly perturbed pathway. Notably, raffinose supplementation (10% w/v) recapitulated radiation-induced microbiota shifts and delayed bone marrow recovery. Fecal microbiota transplantation (FMT) revealed a causative role for raffinose-metabolizing microbiota, particularly *Bacteroides acidifaciens*, in delaying RAHR progression. Mechanistically, *B. acidifaciens*-mediated bile acid deconjugation activated FXR, subsequently suppressing NF-κB-dependent hematopoietic recovery. Therapeutic FXR inhibition *via* ursodeoxycholic acid (UDCA) had been shown to be a viable method for rescuing RAHR. Our results delineated a microbiome-bile acid-FXR axis as a master regulator of post-irradiation hematopoiesis. Targeting *B. acidifaciens* or its metabolic derivatives could represent a translatable strategy to mitigate radiation-induced hematopoietic injury.

ARTICLE HISTORY
Received 20 December 2024
Revised 23 March 2025
Accepted 28 March 2025

KEYWORDS
Radiation-induced hematopoietic injury; gut microbiome; *Bacteroides acidifaciens*; raffinose-metabolizing bacteria; Intestinal-Hematopoietic Axis; UDCA; FXR

Introduction

Exposure to high doses of ionizing radiation (IR) over a brief period can lead to the onset of acute radiation syndrome (ARS),[1] which manifests in various forms, with the hematopoietic subsyndrome (HS) being the most prevalent,[2,3] followed by gastrointestinal subsyndrome (GIS), neurovascular subsyndrome (NVS), and cutaneous subsyndrome (CS). These subsyndromes are categorized based on the IR dose, associated pathology, and clinical course.[2] The severity of hematopoietic damage and the extent of recovery profoundly influence the progression and outcome of HS.[2] Hematopoietic stem cells (HSCs), with their self-renewal capabilities, are crucial for hematopoietic recovery.[4] Several therapeutic strategies targeting HSC production or differentiation have shown clinical promise in managing radiation-associated hematopoietic recovery (RAHR).[5–8] However, current therapeutic regimens mainly offer symptomatic relief, failing to target RAHR's multifactorial pathophysiology.

CONTACT Depei Wu wudepei@suda.edu.cn Department of Hematology, The First Affiliated Hospital of Soochow University, 188 Shizi Street, Suzhou 215006, China; Zhemin Zhou zmzhou@suda.ed29u.cn MOE Key Laboratory of Geriatric Diseases and Immunology, Cancer Institute, Suzhou Medical College, Soochow University, 1 Renai Road, Suzhou 215123, China; Xiaofei Qi qixf-sz@hotmail.com Department of Hematology, The First Affiliated Hospital of Soochow University, 188 Shizi Street, Suzhou 215006, China

*These authors contribute equally to this work and should be considered co-first authors.

Supplemental data for this article can be accessed online at https://doi.org/10.1080/19490976.2025.2488105

The gut microbiome, the body's largest symbiotic system, has gained significant attention recently for its crucial role in maintaining internal environmental homeostasis.[9,10] Extensive research has revealed the association between microbiome dysregulation and a wide spectrum of diseases, including Alzheimer's disease,[11] diabetes,[12] and cancer.[13] Consequently, novel therapeutic interventions, including fecal microbiota transplantation (FMT), probiotic supplementation, and pharmacological interventions have emerged to restore gut microbiome balance,[14–16] offering therapeutic potential for these conditions. Microbiome-based therapy holds great promise in the management of RAHR, but our understanding of the role of bacteria in radiation injury remains limited.

Recent interest had focused on the characteristic changes of gut microbiota and their metabolites in ARS,[17] yet the precise relationship between gut microbiota and RAHR remained unclear. To address this gap, an RAHR mouse model was developed, and a comprehensive analysis of the gut microbiome was conducted. Subsequently, we performed in-depth functional and mechanistic studies to elucidate the underlying mechanisms and explore potential therapeutic strategies for mitigating RAHR. Our findings underscored the importance of raffinose-metabolizing bacteria, particularly *Bacteroides acidifaciens*, in delaying bone marrow recovery *via* a bile acid-dependent pathway, and proposed a microbiome-targeted therapeutic strategy for managing RAHR.

Results

Gut microbiome shifts induced by total body irradiation

To explore the correlation between the gut microbiome and disease progression, an HS mice model was established using varying doses of TBI. Mice exposed to 3 Gy of X-ray TBI survived, whereas 6 Gy irradiation induced 100% mortality within 9 d (Supplement Figure S1a). The 3 Gy group exhibited gradual weight loss and decreased white blood cell (WBC) counts in peripheral blood, both reaching their lowest values on the third-day post-irradiation, followed by gradual recovery (Supplement Figure S1bc). Bleeding and severe bone marrow damage were evident within the first 3 d, with a gradual recovery over 2–3 weeks. In contrast, mice exposed to 6 Gy TBI experienced progressive weight loss and severe, irreversible bone marrow damage, ultimately leading to fatality (Supplement Figure S1d).

We employed the 16S rRNA gene sequencing to elucidate the gut microbiome shifts in the HS model. The phylogenetic diversity (faith-PD) of fecal samples decreased significantly after IR exposure (Supplement Figure S2a). At the family level, *Bacteroidaceae* and *Erysipelotrichaceae*, both among the 15 most abundant taxa, increased on the first day post-3 Gy TBI, then declined by the 14th day. In contrast, *Murbaculaceae* and *Prevotellaceae* followed the opposite trend (Supplement Figure S2b). Linear discriminant analysis effect size (LEfSe) analysis corroborated these observations (Supplement Figure S2c). Genus-level analysis revealed rapid enrichment of *Bacteroides, Escherichia-Shigella, Monoglobus, Enterococcus, Faecalibaculum, Dubosiella, Mucispirillum*, and *Helicobacter* post-irradiation, with gradual recovery after the 14th day (Supplement Figure S3a). Notably, *Bacteroidaceae* was the only family enriched on the first day post-exposure to both 3 Gy and 6 Gy irradiation (Supplement Figure S3b).

Concordant microbiome variation in cecal contents

We further analyzed the cecal contents of mice following exposure to 3 Gy and 6 Gy TBI. A decrease in microbial abundance was observed in the cecal contents after 3 Gy TBI, reflecting radiation-induced alterations (Supplementary Figure S4A). Additionally, *Enterobacteroidaceae* and *Bacteroidaceae* exhibited gradual enrichment over time, with the most significant increase observed on the third day post-3 Gy TBI (Supplementary Figure S4b). LEfSe analysis at the genus level revealed consistent enrichment of *Bacteroides* and *Escherichia-Shigella* over time following 3 Gy TBI (Supplementary Figure S4c). Notably, *Bacteroides* exhibited gradual enrichment on the first and third days post-6 Gy TBI, along with *Helicobacter* (Supplementary Figure S4d).

These findings collectively highlighted distinct microbiome alterations following irradiation. By integrating sequencing results from both fecal and

cecal samples, our data demonstrated that the dynamic changes in *Bacteroidetes* were consistent across all experimental conditions and correlated with the progression of bone marrow injury.

Post-radiation enrichment of Bacteroides *in clinical samples*

To investigate the clinical relevance of these observations, we collected fecal samples from seven pelvic cancer patients before and 5 weeks after radiotherapy. We observed a significant post-radiotherapy increase in *Bacteroides* abundance in five patients, consistent with the patterns identified in our murine models (Supplement Figure S2D).

These results provided novel insights into the distinctive shifts in gut microbiome composition induced by irradiation in both murine models and pelvic cancer patients. The consistent enrichment of *Bacteroides* after radiation exposure highlighted the potential link between these microbial changes and radiation-related effects.

Increased raffinose metabolism in gut microbiome of HS mice

To investigate the functional implications of gut microbiota alterations during the progression of IR-induced HS, we used PICRUSt2 software for functional prediction of gut microbiome data. KEGG pathway analysis revealed significant disruptions in amino acid, lipid, polysaccharide, and saccharide metabolism pathways, driven by IR-enriched bacterial populations (Supplement Figure S5a). Among these, pathways related to polysaccharide and saccharide metabolism, particularly raffinose metabolism, were notably affected in mouse fecal samples 1-d post-exposure to 3 Gy TBI (Supplement Figure S5a) and in cecal contents 3-d post-exposure (Figure 1a).

To validate these findings, we conducted an *in vitro* assay to measure saccharide degradation in the feces of HS mice. Of the five saccharides tested, only raffinose exhibited a notable increase in degradation rate 1-d post-3 Gy TBI, followed by a decrease at 21 d (Figure 1b), mirroring the gut microbiome changes in HS mice. Conversely, no significant changes were observed in the degradation rates of the other four saccharides (Supplement Figure S5b). Furthermore, we compared the gene profiles related to raffinose metabolism and found an early accumulation of these genes after radiation exposure. Specifically, in the cecal contents, genes encoding β-fructofuranosidase (K01193) and α-galactosidase (K07406, K07407) gradually increased following TBI (Figure 1c). In fecal samples, α-galactosidase (K07406) peaked 1 d after TBI and then decreased by the 14th day (Figure 1d).

These findings suggested that the enrichment of gut microbiota following irradiation contributed to alterations in raffinose metabolism, potentially playing a key role in the progression of RAHR.

Role of raffinose metabolism in RAHR

To evaluate the role of raffinose-metabolism bacteria in RAHR, we fed mice with drinking water containing 0%, 1%, or 10% raffinose for 1 week. Histological examination revealed no significant differences in raffinose-treated and untreated (0%) groups in major organs (Supplement Figure S6A). However, following exposure to 6 Gy TBI, mice fed with 1% or 10% raffinose exhibited reduced weights compared to untreated controls (Supplement Figure S6c). Additionally, mice fed with 10% raffinose exhibited reduced survival time (Supplement Figure S6b) and thus selected for all subsequent experiments.

After exposure to 3 Gy X-ray TBI, both raffinose-treated and untreated mice displayed similar histological impacts in the liver, spleen, and intestines (Supplement Figure S7), as well as comparable body weight changes (Supplement Figure S8A). However, they differed in the recovery process. The raffinose-treated mice showed a significant decrease in the hematopoietic area of the bone marrow by the third day post-TBI (Figure 2a,b). By day 7, these mice showed severe bone marrow damage, while most untreated mice had fully recovered (Figure 2a,b). Immunohistochemical analysis demonstrated that there was minimal activation of apoptosis in the bone marrow, with only a very small number of cells positive for cleaved caspase-3 (apoptosis marker) at day 3 post-TBI. In contrast, ferroptosis markers exhibited temporal divergence: GPX4 (ferroptosis marker) expression was comparable with

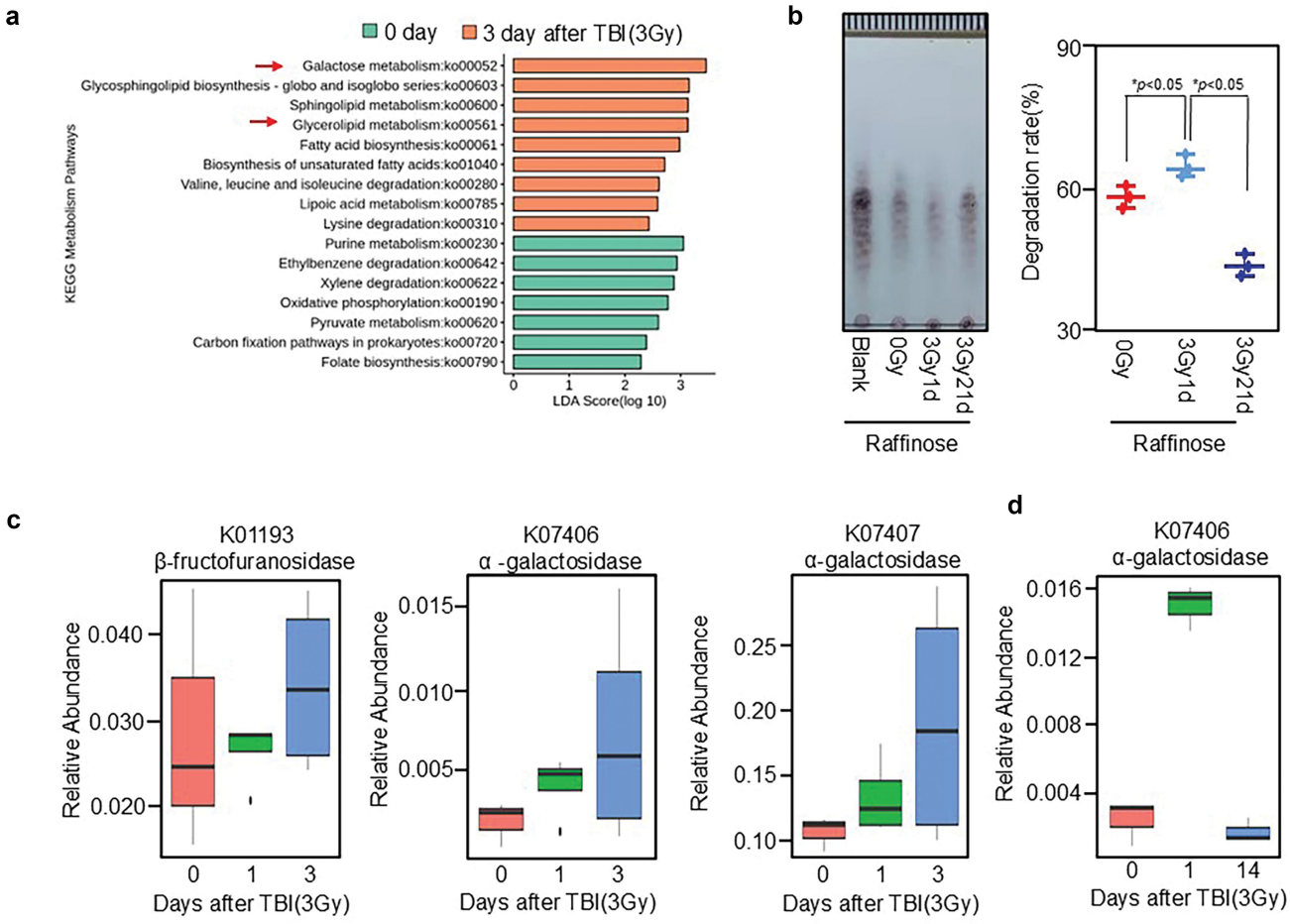

Figure 1. Enrichment of raffinose metabolism in gut microbiome of HS mice. (a) LEfSe analysis of KEGG pathways in mouse cecal contents at 0- and 3-d post-exposure to 3 Gy TBI. Red arrows indicate pathways involved in raffinose metabolism. (b) Raffinose degradation rate detected by raffinose degradation assay with mouse feces samples at 0-, 1-, and 21-d post-exposure to 3 Gy TBI. Medium without feces added used as a blank control (blank) ($n = 3$), the values were representative of data from three independent experiments. (c) Abundance of raffinose metabolism-related genes β-fructofuranosidase (K01193), α-galactosidase (K07406), and α-galactosidase (K07407) in the cecal contents of mice at 0-, 1-, and 3-d post-exposure to 3 Gy TBI. (d) Raffinose metabolism gene α-galactosidase (K07406) abundance in mouse feces samples at 0-, 1-, and 14-d post-exposure to 3 Gy TBI.

these groups at day 3, but the raffinose-treated mice retained elevated GPX4$^+$ cells by day 7 post-TBI, suggesting delayed resolution of ferroptotic stress (Supplement Figure S8d,e).

We investigated the impact of raffinose treatment on hematopoietic stem cells (HSCs), which were responsible for bone marrow recovery. Consistent with the histological findings, no significant difference in hematopoietic stem/progenitor cells (quantified as Lineage$^-$ Sca-1$^+$ c-Kit$^+$ (LSK$^+$) populations) was observed between raffinose-treated and untreated mice by day 3 post-TBI. However, by day 7 post-TBI, untreated mice exhibited about a 40-fold increase in hematopoietic stem/progenitor cells (LSK$^+$ populations) compared to day 3 (208 ± 63 *vs* 5 ± 1 cells, $p < 0.05$). Strikingly, on day 7, mice treated with raffinose showed a significant suppression in both the absolute counts of LSK$^+$ cells (24 ± 10 *vs* 208 ± 63 cells in the untreated group, $p < 0.05$) and the percentage of LSK$^+$ cells among total live cells ($0.114\% \pm 0.014\%$ *vs* $0.393\% \pm 0.064\%$ in the untreated group, $p < 0.05$) (Figure 2c, Supplement Figure S8b). Peripheral blood analysis also revealed lower lymphocyte counts in the raffinose-treated group (Supplement Figure S8c). Interestingly, fecal microbiota analysis showed that raffinose-treated, unirradiated mice had a microbiome composition similar to that of irradiated mice, characterized by a marked enrichment of *Bacteroides* species (Supplement Figures S9a and b).

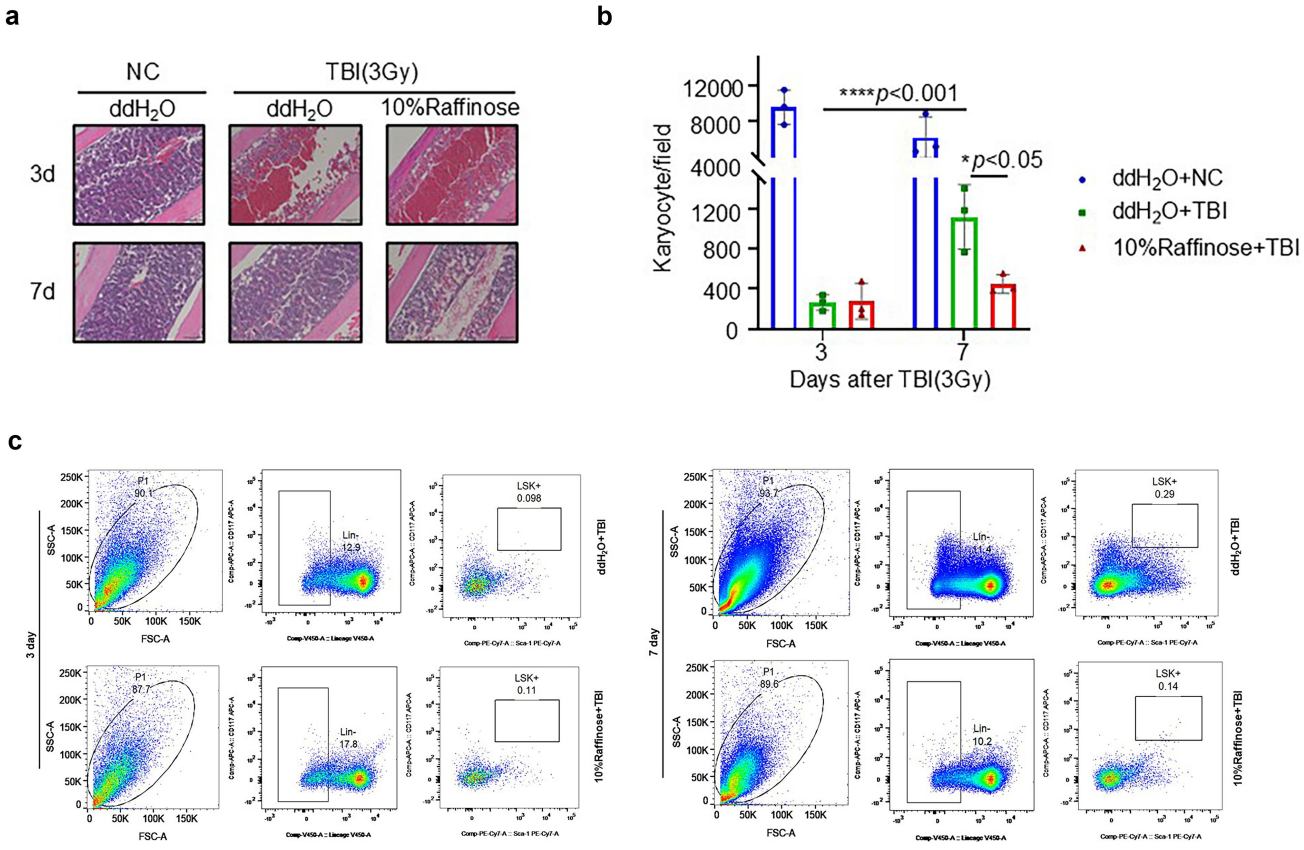

Figure 2. Role of raffinose metabolism in RAHR. (a) Histological examination of mouse bone marrow following TBI with or without raffinose treatment. Mice without TBI served as NC (negative control). (b) Quantification of hematopoietic area in mouse bone marrow on days 3 and 7 post-TBI. Mice without TBI served as NC. (c) FACS analysis of hematopoietic stem cells (LSK^+ cells) in mouse bone marrow with or without raffinose treatment on days 3 and 7 post-TBI. ($n \geq 3$), the values were representative of data from three independent experiments.

These findings suggested that raffinose treatment induced changes in the gut microbiota similar to those seen after radiation exposure, leading to delayed recovery following irradiation. This underscores the regulatory role of raffinose metabolism on the hematopoietic recovery process after radiation.

Gut microbiota mediates raffinose-induced prolonged recovery

To investigate the role of gut microbiome in the raffinose-induced delay of RAHR, we conducted fecal microbiota transplantations (FMT). Fecal samples from raffinose-treated (RD) and untreated (UD) donor mice were transplanted into antimicrobial-treated recipient mice, resulting in two recipient groups of RR (FMT from RD) and UR (FMT from UD) (Figure 3a).

Following TBI treatments, all mice initially experienced similar weight loss and bone marrow damage by the third day after 3 Gy (Supplement Figure S10a) and 6 Gy X-ray TBI (Supplement Figure S10b). By the seventh day, however, distinct recovery patterns were observed. The UD and UR mice both showed the most favorable recovery, while RD and RR mice displayed persistent hemorrhages in the bone marrow cavities, which continued even on day 14 post-TBI (Figure 3b, Supplement Figure S10d). Additionally, RD and RR mice had lower white blood cell counts in peripheral blood by the seventh day post-TBI (Supplement Figure S10c). After 6 Gy TBI, RD and RR mice also demonstrated a trend toward shortened survival time compared to the UD and UR groups (Figure 3c). Notably, RR mice, which were not treated with raffinose but received

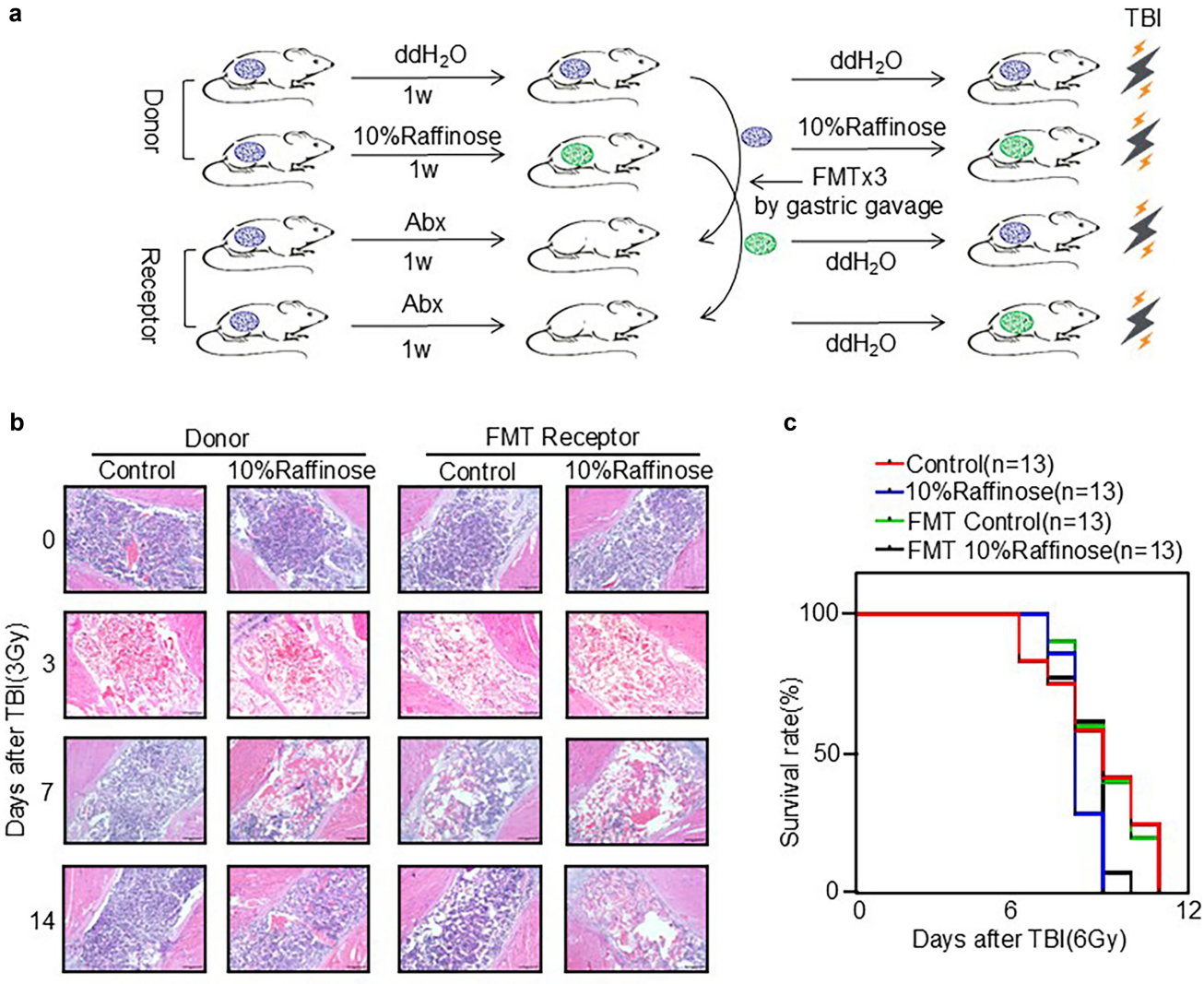

Figure 3. Role of gut microbiota in raffinose metabolism during RAHR. (a) Schematic overview of fecal microbiota transplantation (FMT) protocol. (b) Histological examination of bone marrow in fecal microbiota donor and receiver mice on days 0, 3, 7, and 14 post-TBI. Mice without 10% raffinose treatment served as controls. (c) Assessment of overall survival (OS) in fecal microbiota donor and receiver mice following 6 Gy TBI.

FMT from raffinose-treated donors, exhibited similar delayed recovery as the raffinose-treated mice. This strongly supports the hypothesis that gut microbes play a crucial role in the raffinose-induced delay in RAHR.

Bacteroides acidifaciens responsible for the metabolizing of raffinose inhibit RAHR

Bacteroidetes, or more specifically genus *Bacteroides*, were significantly enriched after both radiation and raffinose treatments. *Bacteroides* are common in the gut microbiome and encompasses dozens of species, including some with strong raffinose-metabolic abilities. These species likely contribute to the raffinose-induced RAHR delay in the murine model. To identify the specific species, we reanalyzed the 16S rRNA sequencing data from fecal samples collected with or without raffinose treatment, focusing on amplicon sequence variants (ASVs).

We identified nine ASVs from the *Bacteroides* genus with significant variations in abundance among the top 200 ASVs. Using a maximum-likelihood phylogenetic analysis of these nine ASVs alongside known *Bacteroides* species, the three ASVs were clustered within the *B. acidifaciens* clade (Figure 4a). These ASVs were notably enriched at 3 and 7 d post-TBI and raffinose treatment

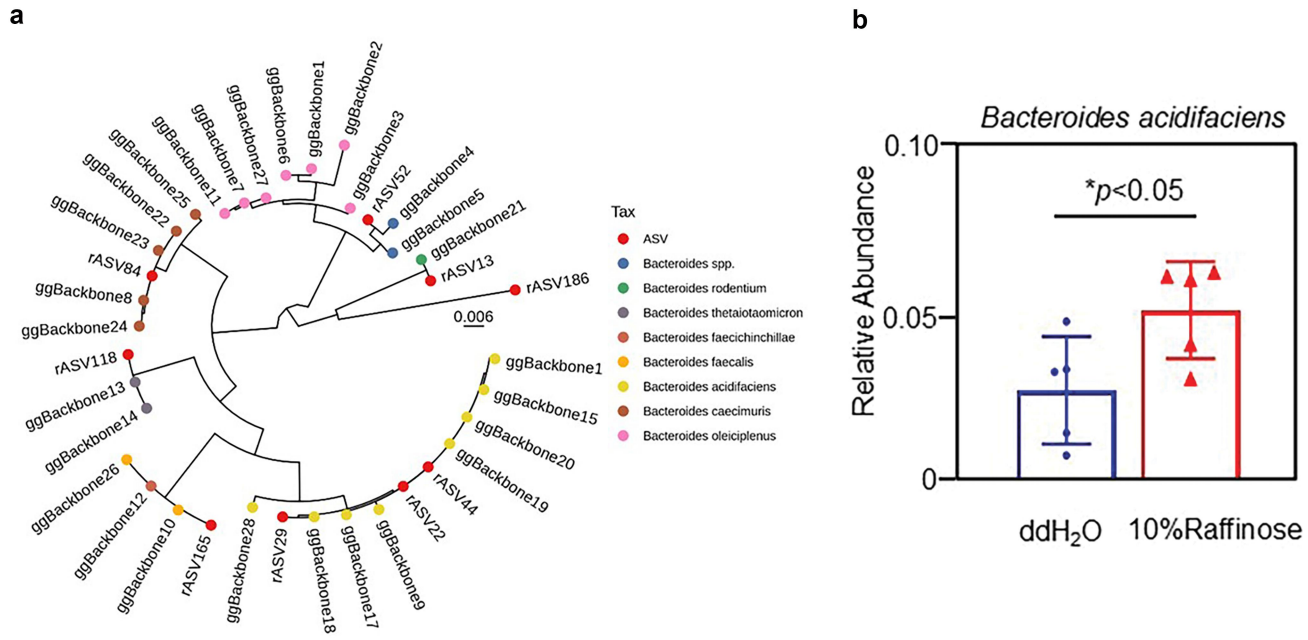

Figure 4. *Bacteroides acidifaciens* as the primary enriched group in raffinose metabolism. (a) Phylogenetic tree *bacteroides spp*. and ASVs. (b) Detection of *Bacteroides acidifaciens* in mouse feces samples with or without 10% raffinose treatment.

(Supplementary Figure S11). Further validation using real-time PCR confirmed the increased abundance of *B. acidifaciens* after raffinose induction (Figure 4b).

To investigate the role of *B. acidifaciens* in RAHR, we administered *B. acidifaciens* to mice *via* gastric gavage before TBI (Figure 5a). Mice treated with raffinose or gavaged with *B. acidifaciens* exhibited significantly reduced survival times compared to controls. Moreover, the combination of raffinose treatment and *B. acidifaciens* gavage led to the worse survival outcomes (Figure 5b). Consistent with our hypothesis, bone marrow recovery was delayed in mice treated with raffinose alone, *B. acidifaciens* alone, or the combination of both, compared to control mice at 7 and 14 d post-TBI (Figure 5c) (Supplement Figure S12). Flow cytometry analysis revealed that untreated control mice had higher numbers of LSK^+ cells compared to those treated with raffinose alone, *B. acidifaciens* alone, or both at 14 d post-TBI (Figure 5d).

In summary, these findings suggested that *B. acidifaciens*, through its role in raffinose metabolism, may inhibit hematopoietic recovery following radiation exposure.

FXR alleviates the delayed impact of raffinose-metabolizing bacteria on RAHR

The farnesoid X receptor (FXR), a key metabolic regulator of bile acids (BAs),[18] could play a crucial role in the modulation of hematopoietic recovery after radiation-induced injury. In $FXR^{-/-}$ mice, there was no significant alteration in the degradation rate of raffinose following IR induction (Figure 6a), and *B. acidifaciens* levels remained unchanged, regardless of radiation exposure (Supplementary Figure S13). This indicated that FXR is integral to the raffinose-metabolizing bacteria's effects on RAHR.

To further explore this, we conducted FMT experiments using $FXR^{-/-}$ or $FXR^{+/+}$ donor mice (Figure 6b). Mice receiving feces from $FXR^{-/-}$ donors had higher numbers and percentage of LSK^+ cells compared to those receiving feces from $FXR^{+/+}$ donors on the seventh day after 3 Gy TBI (Figure 6c,d, Supplementary Figure S14). This suggested that the deletion of FXR mitigated the delayed recovery of bone marrow caused by raffinose-metabolizing bacteria.

Furthermore, we investigated the role of FXR using ursodeoxycholic acid (UDCA), an FXR inhibitor. Mice were divided into groups fed with 10%

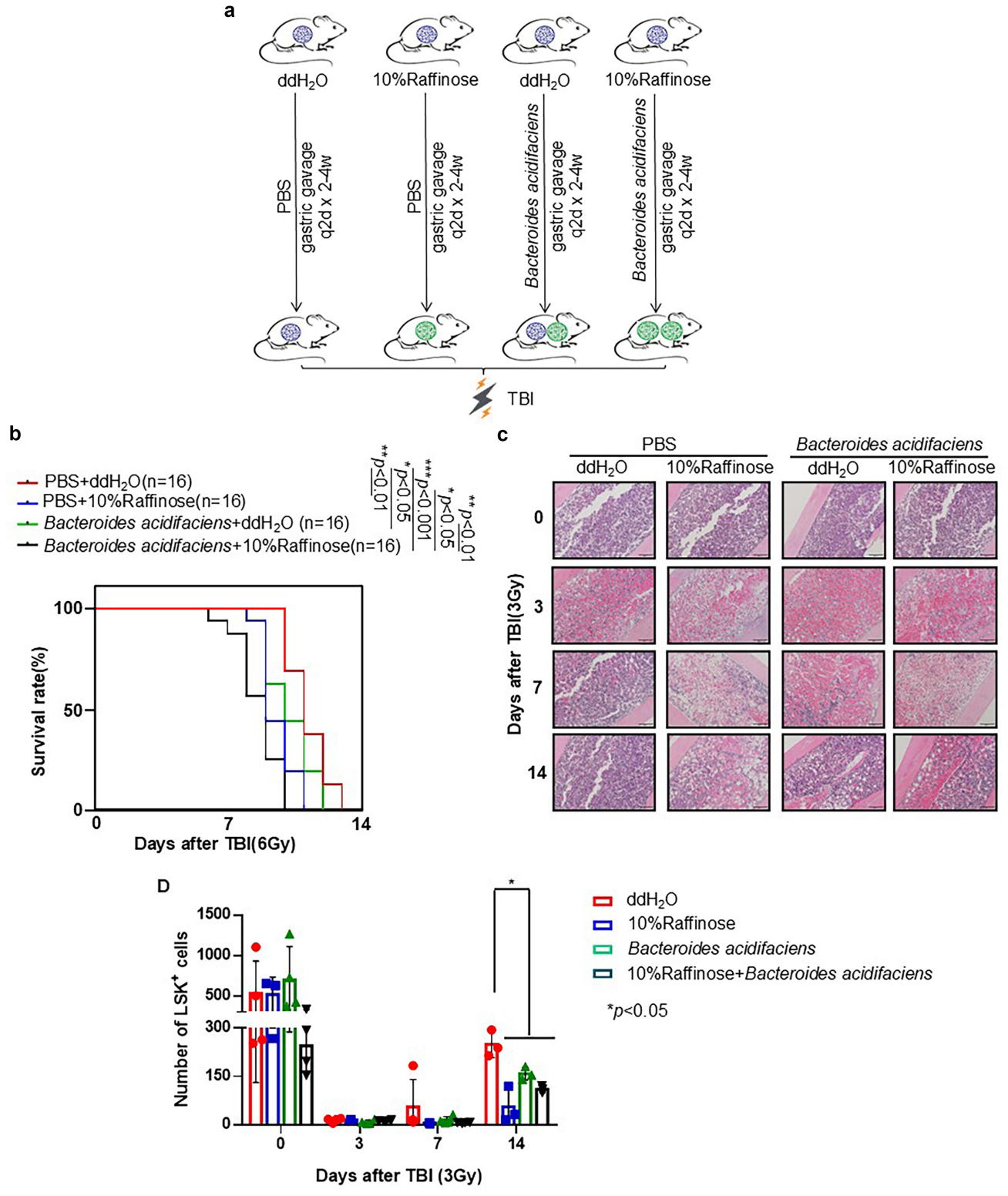

Figure 5. *Bacteroides acidifaciens* responsible for the metabolizing of raffinose inhibit RAHR. (a) Schematic overview of *bacteroides acidifaciens* transplantation protocol. (b) Survival curves in mice following 6 Gy TBI. (c) histological examination of bone marrow on days 0, 3, 7, and 14 post-3 Gy TBI in mice with or without *Bacteroides acidifaciens* transplantation. d. Detection of LSK^+ cells on days 0, 3, 7, and 14 post-3 Gy TBI in mice with or without bacteroides acidifaciens transplantation. ($n \geq 3$), the values were representative of data from three independent experiments.

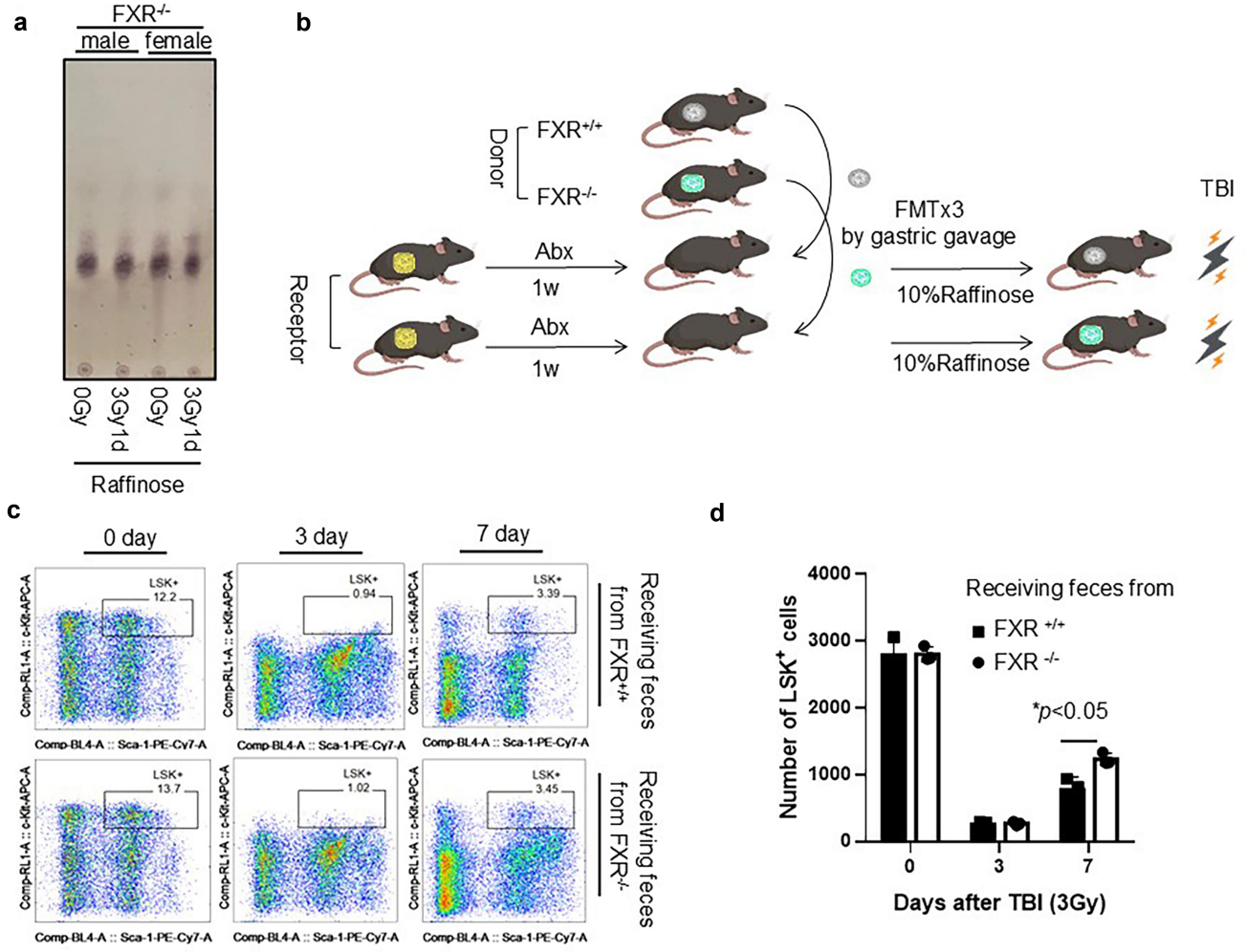

Figure 6. FXR pathway could alleviates the delayed impact of raffinose-metabolizing bacteria on RAHR. (a) Raffinose degradation rate of FXR knockout mice feces samples following 3 Gy TBI exposure (b) Schematic of fecal microbiota transplantation using FXR knockout or wild-type mice feces as donors. (c) Detection of LSK^+ cells in receiver mice on days 0, 3, and 7 post-3 Gy TBI. (d) Quantification of the number of LSK^+ cells in recipient mice on days 0, 3, and 7 post-3 Gy TBI. ($n \geq 3$), the values were representative of data from three independent experiments.

raffinose, 10% raffinose+UDCA, ddH_2O+UDCA, or only ddH_2O as a control. Antimicrobial-treated mice were transplanted using feces from these mice, followed by 3 Gy TBI (Figure 7a). Mice transplanted by feces from 10% raffinose-fed donors exhibited significantly lower LSK^+ cells counts and percentages compared to controls on the seventh day post-TBI. However, treatments with 10% raffinose+UDCA, or UDCA alone, exhibited normal LSK^+ cells levels, demonstrating that inhibition of FXR rescued hematopoietic recovery (Figure 7b, Supplementary Figure S15).

Bile acid metabolites/FXR/NF-κB were crucial for RAHR inhibition by raffinose-metabolizing bacteria

Raffinose-metabolizing bacteria, particularly *B. acidifaciens*, appeared to inhibit RAHR through FXR-related mechanisms involving bile acid metabolism. *In vitro* assays confirmed that *B. acidifaciens* elevated the proportion of deconjugated bile acids, irrespective of the origin (human or mouse) of the bile acids (Figure 8a,b, Supplementary Figure S16).[19–21] The deconjugated bile acids act as FXR agonists,[22] implicating FXR activation during IR or raffinose treatment.

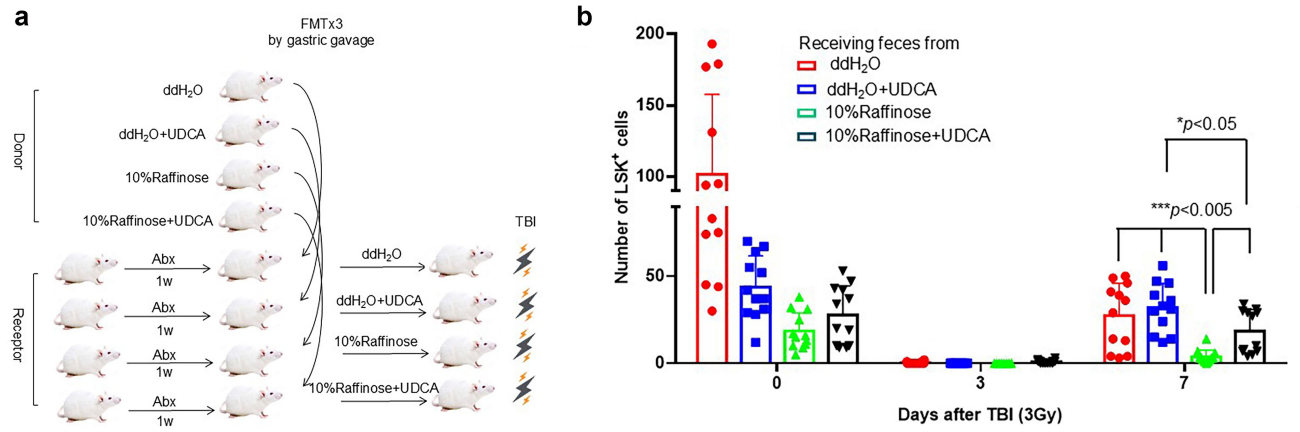

Figure 7. UDCA, an FXR Inhibitor, facilitates hematopoietic recovery *via* gut bacteria. (a) Schematic of fecal microbiota transplantation using feces from mice treated with or without UDCA as donors. (b) Quantification of the number of LSK^+ cells in recipient mice on days 0, 3, and 7 post-3 Gy TBI. ($n \geq 3$), the values were representative of data from three independent experiments.

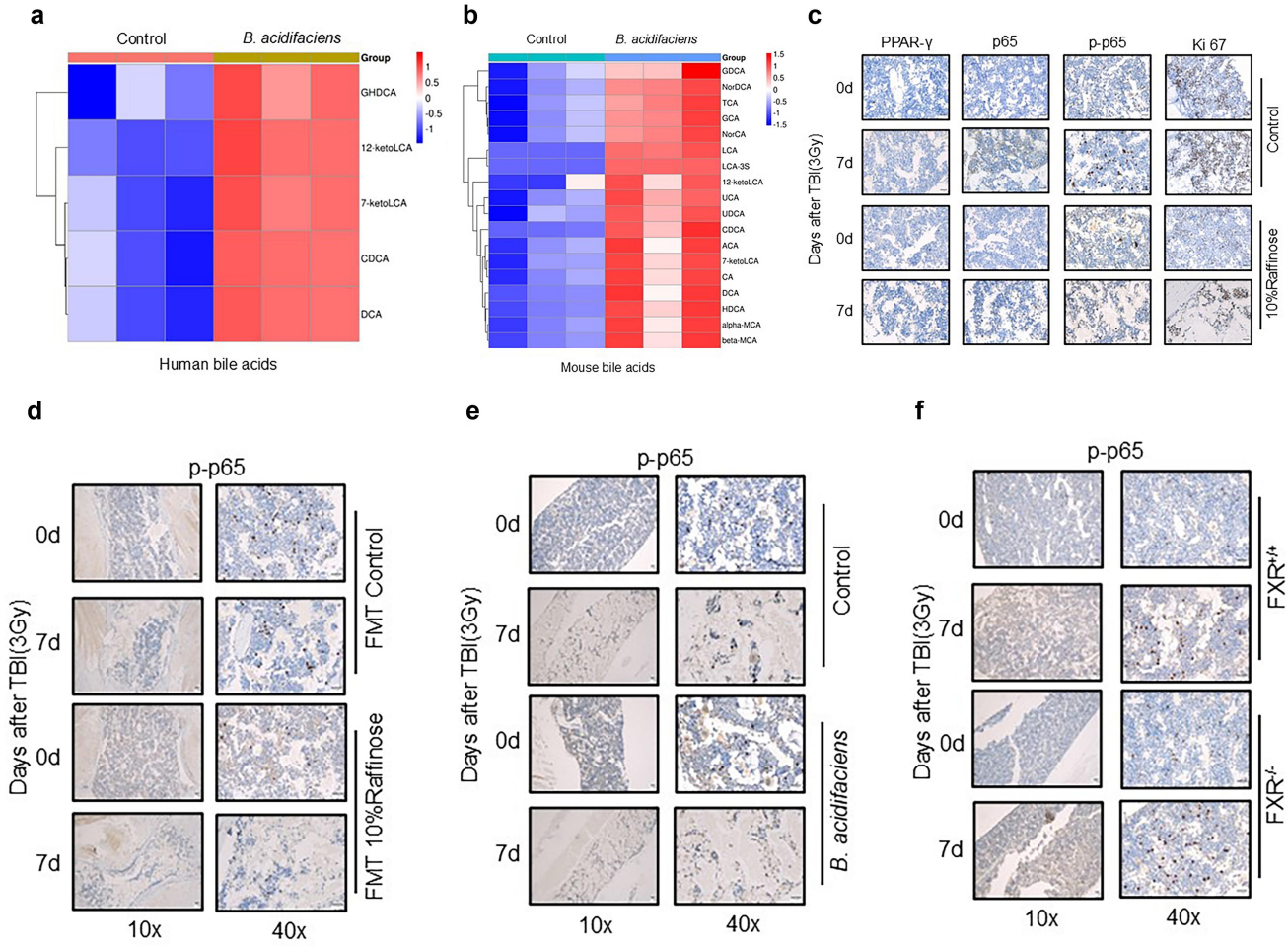

Figure 8. Raffinose-metabolizing bacteria inhibit RAHR through bile acid metabolites/FXR/NF-κB pathways. (a) Marked alterations in human bile acid profiles *in vitro* treatment with *B. acidifaciens*. Each column represents a sample. (b) Marked alterations in mouse bile acid profiles *in vitro* treatment with *B. acidifaciens*. Each column represents a sample. (c) Detection of PPAR-γ, p65, p-p65, and Ki67 in mouse bone marrow following TBI with and without raffinose treatment, immunohistochemical analysis of tissue sections from Figure 2a (40×). (d) Detection of p-p65 in fecal microbiota receiver mice bone marrow on days 0, 7 post-TBI, immunohistochemical analysis of tissue sections from Figure 3. (e) Detection of p-p65 in mice bone marrow on days 0, 7 post-TBI with and without *B. acidifaciens*. treatment, immunohistochemical analysis of tissue sections from Figure 5. (f) Immunohistochemical analysis of p-p65 in $FXR^{+/+}$ and $FXR^{-/-}$ mice bone marrow on days 0, 7 post-TBI.

To examine the downstream effects of FXR activation, we focused on the expression of NF-κB and PPAR-γ, two crucial proteins influenced by FXR.[20,23–25] We observed that p65, a subunit of NF-κB, was significantly activated post-IR in both raffinose-treated and untreated mice, but there was no significant difference between the two groups. Notably, we observed elevated levels of phosphorylated p65 (p-p65) in the bone marrow of untreated mice, indicating NF-κB activation. However, in raffinose-treated mice, p-p65-positive cells were scarce both before and after irradiation (Figure 8c, Supplementary Figure S17a). Similarly, the untreated mice also exhibited a higher proportion of Ki67-positive cells post-IR (Figure 8c, Supplementary Figure S17b). This trend was consistent in mice receiving FMT from raffinose-treated donors (Figure 8d, Supplementary Figure S17c), and in those treated with *B. acidifaciens* alone or in combination with raffinose post-IR (Figure 8e). Notably, FXR knockout mice did not exhibit significant differences in the number of p-p65-positive cells post-TBI compared to $FXR^{+/+}$ mice, further emphasizing FXR's role in regulating NF-κB activity and its downstream impact on RAHR (Figure 8f, Supplementary Figure S17d).

These findings revealed that raffinose-metabolizing bacteria, such as *B. acidifaciens*, disrupted bile acid metabolism and modulated FXR activity, thereby influencing hematopoietic recovery post-radiation through inhibition of NF-κB activation.

Discussion

The restoration of hematopoietic function was crucial for mitigating IR-induced damage.[1] While clinical treatments such as hematopoietic growth factors and stem cell transplants have demonstrated efficacy,[1,4,5,26] better RAHR management requires a deeper understanding of the underlying mechanisms. HS occurs when high doses of IR cause severe bone marrow damage, resulting in a significant reduction or complete cessation of hematopoiesis.[8] In this study, we established an HS mouse model using male BALB/c mice, known for their radiation sensitivity.[27] Following exposure to 3 Gy X-ray TBI, the mice exhibited classic HS phenotypes, including bone marrow damage, weight loss, and reduced peripheral blood leukocyte counts. These phenotypes peaked in severity by the third day post-TBI and gradually improved, indicating the progression and recovery from HS. Furthermore, exposure to 6 Gy X-ray TBI resulted in 100% mortality in 8–12 d, confirming the lethality at this dose. Therefore, this model was suitable for investigating the relationship between the gut microbiome and RAHR.

The gut microbiome interacted with intestinal microenvironment and/or nutrients and played important physiological roles *via* remote effects,[10] including the Intestinal-Hematopoietic Axis investigated here. Radiation exposure resulted in significant disturbances in the gut microbiome, notably reducing taxonomic diversity, a phenomenon previously associated with both IR exposures[28,29] and elevated bile acid levels[30] in mice and humans. Notably, we evidenced a consistent enrichment of *Bacteroides* in the cecal and fecal samples of mice subjected to either 3 Gy or 6 Gy TBI. Consistent with our results, there were many papers reported that *Bacteroidetes* were enriched under 3 Gy, 4 Gy, and 6 Gy irradiation.[31,32] This bacterial shift was coupled with a functional increase in raffinose-metabolizing genes post-TBI, suggesting a direct role of *Bacteroides* in the RAHR process.

Raffinose is a natural functional oligosaccharide, a galactose/fructose/glucose trisaccharide, and a soluble dietary fiber and is widely found in plant seeds, fruits, rice, and oilseeds.[33,34] Not absorbed or degraded in the upper gastrointestinal tract, raffinose reaches the large intestine, where it is fermented by microbes.[35] While raffinose is often described as prebiotics, our findings highlight its negative impact on RAHR in mice. Mice fed with raffinose demonstrated delayed recovery of the hematopoietic area after 3 Gy TBI and reduced survival after 6 Gy TBI. These results align with clinical observations, where increased sensitivity to radiation has been reported in patients supplemented with soluble fiber, which contains high levels of raffinose,[36] underscoring the associations between raffinose and IR treatments.

Our findings further demonstrated that gut microbiome plays an essential role in the delayed RAHR caused by raffinose. Transplantation of feces from raffinose-treated mice into antibiotic-treated mice resulted in similar delayed RAHR

recovery, even without the administration of raffinose itself. This suggests that gut microbial composition, rather than raffinose alone, mediates this delayed recovery.

Notably, the taxonomic composition of the gut microbiome from raffinose-treated mice resembled that of IR-treated mice, with a significant increase in *Bacteroides* species. Using ASV analysis, we further examined the *Bacteroides* population, identifying nine distinct ASVs. Of these, three ASVs that exhibited increased abundance after both irradiation and raffinose treatment belonged to the *B. acidifaciens* clade in the 16S rRNA phylogeny. Moreover, our *in vivo* tests revealed that mice gavaged with *B. acidifaciens* exhibited delayed RAHR similar to those treated with raffinose, further demonstrating the role of *B. acidifaciens* in the process.

Some previous studies associated raffinose supplement with increases in *Lactobacillus* and *Bifidobacterium* in the gut microbiome.[37] However, consistent with other reports,[28] we did not observe a significant increase in these two genera post-TBI. In fact, *Bifidobacterium* decreased in both fecal and cecal samples post-TBI, while *Lactobacillus* increased in cecal and feces after six and 14 d post-TBI, respectively. The predominant contributor to enhanced raffinose metabolism post-TBI was *B. acidifaciens*, which exerts a modulating effect on the intestinal environment by lowering pH and altering bile acid composition.[19,20,38]

The enrichment of *B. acidifaciens* following raffinose supplementation and radiation exposure led to an increased production of deconjugated bile acids,[20,21] which are potent agonists of the farnesoid X receptor (FXR).[20,22,39] The activation of FXR, a nuclear receptor involved in bile acid homeostasis,[18,40,41] appeared to be the primary driver of the delayed RAHR recovery. FXR activation triggered downstream pathways,[21,42] particularly the inhibition of NF-κB signaling,[22,23,43–45] which was known to regulate inflammatory and immune responses. This, in turn, affected cellular growth and recovery processes,[23,43] likely contributing to the delayed hematopoietic recovery observed in the presence of raffinose-metabolizing bacteria.

To evaluate the hypothesis, we administered raffinose to FXR knockout ($FXR^{-/-}$) mice and found that they did not exhibit increased raffinose metabolism nor delayed RAHR recovery after raffinose treatment. Additionally, similar protective effects were observed in wild-type mice treated with ursodeoxycholic acid (UDCA), an FXR antagonist. These findings substantiate FXR activation as the mechanistic link between bile acids and HSC depletion, as previously suggested by studies on bile acid homeostasis and gut microbiota interaction.[42,46,47] Our results further suggested a bi-directional relationship between *B. acidifaciens* and bile acid, resulting in reduced HSC counts and delayed RAHR recovery. The administration of UDCA not only blocked FXR activation but also rescued the delayed RAHR, positioning it as a potential therapeutic option for HS treatments.

RAHR management, especially the critical restoration of hematopoietic function,[26] presents a complex process involving regulatory pathways, cellular interactions, and, long being underestimated, the gut microbiome. We established a novel gut-liver-bone marrow axis wherein *B. acidifaciens*-mediated raffinose metabolism orchestrated FXR-dependent suppression of hematopoietic recovery through bile acid/NF-κB crosstalk. Treatments involving radiation and raffinose administration significantly increased the abundance of *B. acidifaciens* in the gut microbiome. This microbial augmentation led to higher levels of free bile acids, which subsequently activated FXR. The activation of FXR triggered a suppression of NF-κB signaling and inhibited cellular proliferation, ultimately reducing the number of HSCs and delaying RAHR recovery (Figure 9).

Our study had several limitations. First, it mainly focused on *B. acidifaciens* as the primary raffinose – metabolizing bacterium enriched in both radiation and raffinose treatments, while other microbial species varying under only one condition may also contribute to RAHR. Second, the detailed mechanisms linking *B. acidifaciens* enrichment to elevated bile acid levels need further study. Third, the efficacy of alternative therapies like raffinose restriction or targeted antimicrobials against *Bacteroides* warrants more investigation. Moreover, we lacked data on the dynamic changes of the intestinal flora after 4 Gy and 5 Gy irradiation. The clinical sample size was small, and the follow – up time was inadequate. These issues should be addressed in the future research.

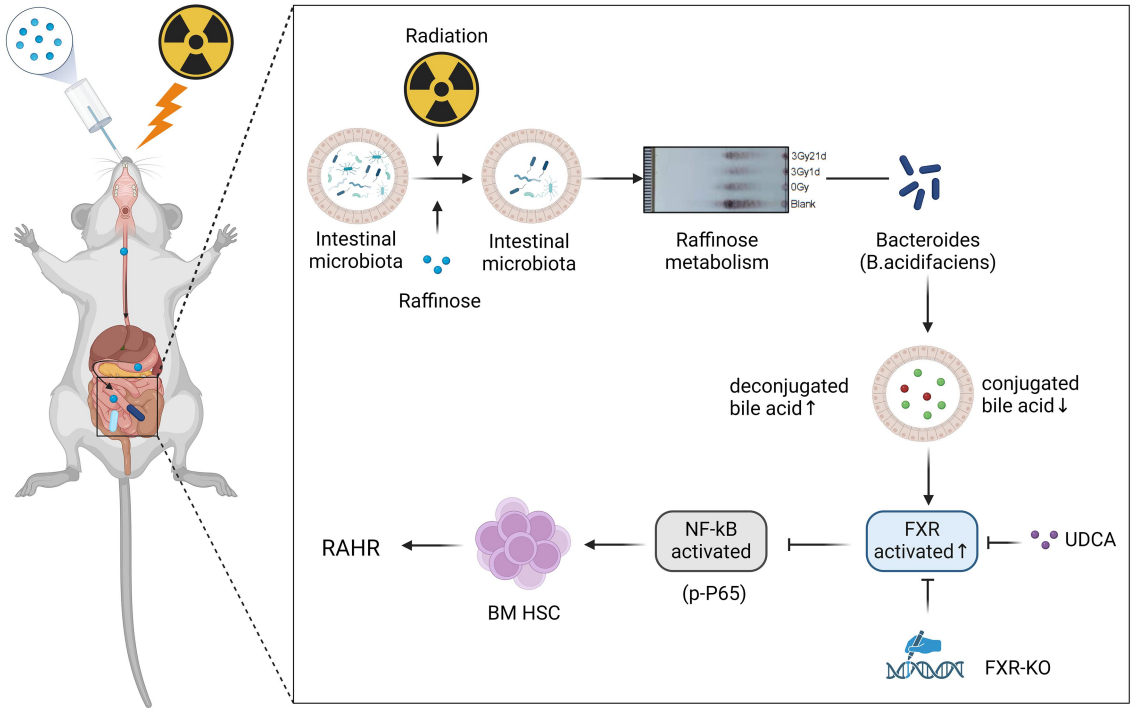

Figure 9. Research graphic Abstracts.

In conclusion, this study suggested that raffinose-metabolizing bacteria, especially *B. acidifaciens*, delay RAHR recovery in a bile acid/FXR/NF-κB pathway. Interventions targeting these bacteria, particularly via FXR inhibition or UDCA administration, offer promise for the prevention and treatment of HS. These findings offered insights into the Intestinal-Hematopoietic Axis and provided new avenues for investigating its role in various diseases, including HS.

Methods

Animals

Male BALB/c and C57BL/6N mice, aged 8 to 10 weeks and weighing 25 ± 3 g, were purchased from Gempharmatech (Nanjing, China). FXR knockout C57BL/6N mice (FXR-/-) were also included in the study, which was constructed by Cyagen Biosciences (Suzhou, China). The genotype of FXR-/- mice was verified by a PCR kit using primers as follows: Primers1: sense 5'-TGTGTTGTATGAGAGTTTTGTCCGC-3', antisense 5'- GATTTGTGGTGTCCTGTATTCC TAG-3'; Primers2: sense 5'- TGTGTTGTATGAG AGTTTTGTCCGC-3', antisense 5'- TGAGCCAA GGGGATGTAGCAATG −3'. Mice were maintained in specific pathogen-free (SPF) facilities at Soochow University's Experimental Animal Center, provided with food and water by the experimental animal center. The housing conditions maintained a room temperature of 20–24°C with a humidity level of 40–60%, while ensuring strict bacterial control. Stringent regulations were in place for the entry and exit of personnel and materials. All animal experiments were conducted following the NIH guidelines and approved protocols by the Institutional Animal Care and Use Committee of Soochow University, with approval from the Animal Ethics Committee of Soochow University.

Clinical samples

The clinical samples were obtained from the Affiliated Jiangyin People's Hospital of Nantong University, and the study was approved by the Ethics Committee of the same hospital in accordance with the Helsinki Declaration. Fecal samples were collected from radiotherapy patients with written informed consent. All cases where patients had used hormones or antibiotics within the three – week period prior to the sampling time point were excluded from the study.

Total body irradiation for HS model construction

To construct the HS mice model, TBI was performed using the RS-2000 Pro biological X-ray irradiator (Rad source, USA) at an average dose rate of 1.225 Gy/min, with a voltage of 160 kV, a current of 25 mA, and a source skin distance of 40 cm.[48] The irradiation time was adjusted based on the desired irradiation dose. After irradiation (IR), the mice were returned to the staging room for further housing and care.

Evaluation of IR-induced hematopoietic injury

Post-irradiated mice were monitored daily for their condition, body weight, and survival. To evaluate hematological changes at different doses and time points, we selected at least three mice from each group on specific days post-irradiation. Blood samples were collected from the orbital venous plexus using a volume of 30 µl and mixed thoroughly with 180 µl of diluent. The cell contents of the blood samples were determined using an automatic animal blood and body fluid analyzer (Sysmex, Japan).

Subsequently, the liver, spleen, and sternum of the mice were collected after IR. The tissues were collected, fixed in a 4% paraformaldehyde solution, decalcified, embedded in paraffin, and proceeded to sections preparation as previously described.[49] Histopathological analysis of the tissue sections was performed using a hematoxylin and eosin (HE) staining kit. The histopathological changes were observed under a microscope (Olympus, Japan). And the lesions of bone marrow were quantitatively analyzed as the number of bone marrow cells and the area of hematopoietic tissue using ImageJ software (National Institutes of Health Image, USA).[50]

16S rRNA amplification and sequencing

Sequencing and analysis were conducted by OE Biotech Co., Ltd. (Shanghai, China). The total genomic DNA was extracted using a DNA Extraction Kit following the manufacturer's instructions. The quality and quantity of the DNA were evaluated using NanoDrop and agarose gel electrophoresis. The extracted DNA was diluted to a concentration of 1 ng/µl and stored at −20°C until further processing. The bacterial 16S rRNA genes were amplified using barcoded primers and Takara Ex Taq (Takara, Japan) with the diluted DNA as the template. The quality of the amplicons was assessed by gel electrophoresis. The amplifications were then purified using AMPure XP beads (Agencourt) and subjected to an additional round of PCR amplification. The final amplicons were quantified using the Qubit dsDNA assay kit. Equal amounts of purified amplicons were subsequently pooled or sequencing. The data structure was optimized for further bioinformatic analysis.

16S rRNA gene sequence analysis

The raw paired-end sequencing data were filtered, merged, and trimmed using Fastp software (v0.22.0).[51] Amplicon sequence variant (ASV) of the 16S rRNA gene sequences was analyzed using the DADA2[52] workflow in the QIIME 2 software[53] (version 2022.4). The ASVs were taxonomically assigned using QIIME2 classify-sklearn workflow based on the Silva 138 database. All the ASVs were filtered by a length of 200 bp. For the radiation exposure only experimental group, the reads count of ASVs of mouse feces samples was rarefied to 14,000 and of mouse gut samples were rarefied to 30,000. For the radiation exposure after 7 d' raffinose culture experimental group, the reads count of ASVs of mouse feces samples was rarefied to 24,000. All the subsequent analyses were based on rarefied ASV table. Based on the rarefied ASV table and sequences, Picrust2[54] was applied to predict the functional profile, and then ggpicrust[55] was used to get the KEGG pathway profile.

The alpha diversity was measured using the Faith PD index which produced by QIIME2 alpha-diversity workflow. LEfSe software[56] was used for detecting group-wise differential features with an LDA score greater than 2. The statistical significance of the differences was determined using the Wilcoxon rank-sum test in R4.3. All the figures were made by ggplot2 and ggpubr package in R4.3.

For getting the *Bacteroides spp*. sequences which were close to *Bacteroides* ASV in this study from public database, we used Greengene2 as a reference and used Vsearch software to searching (–i 0.95). Phylogenetic tree *Bacteroides spp*. was constructed by FastTree after aligned through MAFFT, and ggtree was used to visualize the tree.

Saccharides fermentation and thin-layer chromatography

To evaluate the degradation of saccharides by the gut flora, saccharide fermentation and thin-layer chromatography (TLC) were conducted. Mouse feces were suspended in phosphate-buffered saline (PBS) to create a 10% solution. A 0.5 ml volume of the fecal suspension was then inoculated into the culture medium and incubated in a bacterial incubator at 37°C for 24 h. The saccharide degradation rate was detected using thin-layer chromatography. The preparation of chromogenic chromatography plates involved spotting, unfolding, staining, and other relevant procedures.[57] The plate was then photographed, and the rate of saccharide degradation was quantitatively analyzed using TLC software (Hangzhou Hailu, China).

Flow cytometry assay

The mice were euthanized using sodium pentobarbital and sterilized with 75% alcohol for 5 min. The tibia and femur from the lower limbs were placed aseptically in pre-cooled phosphate-buffered saline (PBS). The bone marrow was aspirated into a 15 ml centrifuge tube containing sterile PBS. The bone marrow cell suspension was then passed through a 200-mesh sieve to eliminate cell clumps. Finally, the cells were resuspended to obtain a single-cell suspension and kept on ice.

The antibodies used for flow cytometry staining were anti-mouse Ly-6A/E (Sca-1) PE-Cy7 (BioGems), anti-mouse CD117 (c-Kit) APC (BioGems), anti-mouse CD34 FITC (BioGems), anti-mouse CD16/CD32 PE (BioGems), and Pacific BlueTM anti-mouse lineage cocktail (BioLegend, USA). The cells were washed with PBS and analyzed using the FACSVerse Cell Analyzer (BD, USA). All data were analyzed using Flowjo software (BD, USA).

Feces microbiota transplantation (FMT)

The mice were randomly divided into donors and recipients. The recipients were given sodium ampicillin (1 g/L), vancomycin (0.5 g/L), neomycin sulfate (1 g/L), and metronidazole (1 g/L) via drinking water, which was replaced every other day for 7 consecutive days. To prepare a suspension, the feces of the donor mice were added to sterile PBS and vortexed followed by filtration through a 200-mesh sterile mesh sieve. After briefly vortexing, the supernatant was collected by centrifugation at 600 g for 5 min and was administered to the recipients by gavage.

Bacterial culture and mono bacterial transplantation

The lyophilized bacterial powder of *Bacteroides acidifaciens* JCM 10,556 was purchased from Ningbo Mingzhou Biotechnology Co., Ltd. and stored at 2–8°C. The culture process required a blood plate culture in a special anaerobic airbag, and an anaerobic glove box was required to ensure an oxygen-free environment for *Bacteroides acidifaciens*.

The bacterial suspension was prepared by centrifuging and resuspending *Bacteroides acidifaciens* in the logarithmic stage, resulting in a concentration of approximately $10^8 \sim 10^9$ cfu/ml. The bacterial liquid sample was diluted and then transplanted via microbial gavage. Gastric gavage transplantation was carried out twice a week, with a colonization cycle of 2 ~ 4 weeks for general single bacteria and a gavage amount of approximately 10 μl/g. The Balb/C male mice were divided into four groups: control, raffinose, *Bacteroides acidifaciens*, and raffinose plus *Bacteroides acidifaciens*. After 2–4 weeks of gavage, the mice were exposed to 3 or 6 Gy TBI.

Quantitative real-time polymerase chain reaction (qRT-PCR)

The qRT-PCR assay was conducted following the previously described method.[49] DNA was extracted from the above clinical feces' samples to detect the concentrations of *Bacteroides*. The qRT-PCR was performed on the Applied Biosystems ViiA7Dx (Life Technologies, America) using *Bacteroides spp*. SYBR qPCR Kit (Tiandz, China).

In vitro *bile acids metabolism assay and mass spectrometry analysis*

To examine *Bacteroides acidifaciens* could affect bile acids metabolism, an *in vitro* bile acids metabolism assay was performed. The strains were inoculated into anaerobic tubes containing Brain Heart Infusion (BHI) medium (Hope Biotech, Shandong, China) for activation and subjected to two consecutive passages for fermentation. Subsequently, 0.5 mL of the bacterial suspension was inoculated into 5 mL of BHI medium supplemented with 5 μL/mL of bile acids derived from either human or mouse sources. This mixture was then subjected to anaerobic fermentation at 37°C for 48 h. Following completion of the fermentation process, the bile acid profile was quantitatively analyzed using Liquid Chromatography-Tandem Mass Spectrometry (LC-MS/MS), which was performed by Hailu Biotech (Hangzhou, China), MS analysis was performed as described in previous study[21,58]

Quantification and statistical analysis

Statistical analysis and data presentation were performed using GraphPad Prism software (GraphPad Software, America). Experimental results were expressed as mean ± standard deviation and tests were repeated three times. Differences between the two groups were analyzed using an independent samples two-sided t-test, with a significance level of $p < 0.05$.

Disclosure statement

No potential conflict of interest was reported by the author(s).

Funding

This study was supported in part by grants from of Foundation of the National Clinical Research Center for Hematologic Disease of China [2020ZKPC01]; the National Key R&D Program of China [2022YFC2503703]; the Priority Academic Program Development of Jiangsu Higher Education Institutions (PAPD) and "333 project" of Jiangsu [BRA2020398]; Project of the State Key Laboratory of Radiation Medicine and Protection, Soochow University [GZN1202101, GZK1202401]; Project of Jiangsu Commission of Health [K2023037]; the Provincial-level Talent Program for National Center of Technology Innovation for Biopharmaceuticals [NCTIB2024JS0101]; the Suzhou Top-Notch Talent Groups [ZXD2022003].

ORCID

Zhemin Zhou http://orcid.org/0000-0001-9783-0366

Author contributions

Z.Z., D.W., and X.Q. designed and supervised the project. Y.J., J.R., N.Y., J.S., H.Y., J.W., J.C., H.G., and X.W. performed and analyzed the experiments. Y.J., H.Y., and J.W. designed and collected the clinical samples. S.X. and Z.Z. contributed to the data analysis. Y.J., Z.Z., D.W., and X.Q. wrote the manuscript. Y.J., J.R., and S.X. contributed equally to the study. All authors approved the manuscript. X.Q. planned and supervised the study, interpreted the experiments, collected all data, and wrote the manuscript. All the authors approved the final manuscript.

Data availability statement

Data of 16S rRNA sequencing have been deposited at https://doi.org/10.6084/m9.figshare.25370296.v1. These data are publicly available as of the date of publication. This paper does not report the original code. All data are available in the main text or the supplementary materials. Correspondence and requests for materials should be addressed to Xiaofei Qi (qixf-sz@hotmail.com)

References

1. Dainiak N, Albanese J. Medical management of acute radiation syndrome. J Radiol Prot. 2022;42(3):42. doi: 10.1088/1361-6498/ac7d18.
2. MacVittie TJ, Farese AM, Jackson Iii WE. A systematic review of the hematopoietic acute radiation syndrome (H-ARS) in canines and non-human primates: acute mixed Neutron/Gamma vs. reference quality radiations. Health Phys. 2020;119(5):527–558. doi: 10.1097/HP.0000000000001319.
3. Tanigawa K. Case review of severe acute radiation syndrome from whole body exposure: concepts of radiation-induced multi-organ dysfunction and failure. J Radiat Res. 2021;62(Supplement_1):i15–i20. doi: 10.1093/jrr/rraa121.
4. Qian L, Cen J. Hematopoietic stem cells and mesenchymal stromal cells in acute radiation syndrome. Oxid Med Cell Longev. 2020;2020:1–10. doi: 10.1155/2020/8340756.
5. Bandekar M, Maurya DK, Sharma D, Sandur SK. Preclinical studies and clinical prospects of Wharton's

jelly-derived MSC for treatment of acute radiation syndrome. Curr STEM Cell Rep. 2021;7(2):85–94. doi: 10.1007/s40778-021-00188-4.
6. Yang E, Choi H, Park JS, Noh YW, Choi CM, Lee WJ, Ko J-W, Kim J. A first-in-human study of KMRC011, a potential treatment for acute radiation syndrome, to explore tolerability, pharmacokinetics, and pharmacodynamics. Clin Transl Sci. 2021;14 (6):2161–2170. doi: 10.1111/cts.13073.
7. Chinnadurai R, Forsberg MH, Kink JA, Hematti P, Capitini CM. Use of MSCs and msc-educated macrophages to mitigate hematopoietic acute radiation syndrome. Curr STEM Cell Rep. 2020;6(3):77–85. doi: 10.1007/s40778-020-00176-0.
8. Kernagis DN, Balcer-Kubiczek E, Bazyar S, Orschell CM, Jackson IL. Medical countermeasures for the hematopoietic-subsyndrome of acute radiation syndrome in space. Life Sci Space Res (Amst). 2022;35:36–43. doi: 10.1016/j.lssr.2022.06.002.
9. Gewin V. Going with the gut to understand diseases. Nature. 2022;602(7897):540. doi: 10.1038/d41586-022-00416-9.
10. Lee JY, Tsolis RM, Baumler AJ. The microbiome and gut homeostasis. Science. 2022;377(6601):eabp9960. doi: 10.1126/science.abp9960.
11. Willyard C. How gut microbes could drive brain disorders. Nature. 2021;590(7844):22–25. doi: 10.1038/d41586-021-00260-3.
12. Seo DO, O'Donnell D, Jain N, Ulrich JD, Herz J, Li Y, Lemieux M, Cheng J, Hu H, Serrano JR, et al. ApoE isoform– and microbiota-dependent progression of neurodegeneration in a mouse model of tauopathy. Science. 2023;379(6628):eadd1236. doi: 10.1126/science.add1236.
13. Takeuchi T, Kubota T, Nakanishi Y, Tsugawa H, Suda W, Kwon AT, Yazaki J, Ikeda K, Nemoto S, Mochizuki Y, et al. Gut microbial carbohydrate metabolism contributes to insulin resistance. Nature. 2023;621(7978):389–395. doi: 10.1038/s41586-023-06466-x.
14. Woelk CH, Snyder A. Modulating gut microbiota to treat cancer. Science. 2021;371(6529):573–574. doi: 10.1126/science.abg2904.
15. Qi X, Li X, Zhao Y, Wu X, Chen F, Ma X, Zhang F, Wu D. Treating steroid refractory intestinal acute graft-vs.-Host disease with fecal microbiota transplantation: a Pilot study. Front Immunol. 2018;9:2195. doi: 10.3389/fimmu.2018.02195.
16. Zhao Y, Li X, Zhou Y, Gao J, Jiao Y, Zhu B, Wu D, Qi X. Safety and efficacy of fecal microbiota transplantation for grade IV steroid refractory GI-GvHD patients: interim results from FMT2017002 trial. Front Immunol. 2021;12:678476. doi: 10.3389/fimmu.2021.678476.
17. Hollingsworth BA, Cassatt DR, DiCarlo AL, Rios CI, Satyamitra MM, Winters TA, Taliaferro LP. Acute radiation syndrome and the microbiome: impact and review. Front Pharmacol. 2021;12:643283. doi: 10.3389/fphar.2021.643283.
18. Xiang D, Yang J, Liu L, Yu H, Gong X, Liu D. The regulation of tissue-specific farnesoid X receptor on genes and diseases involved in bile acid homeostasis. Biomed Pharmacother. 2023;168:115606. doi: 10.1016/j.biopha.2023.115606.
19. Wang H, Wang Q, Yang C, Guo M, Cui X, Jing Z, Liu Y, Qiao W, Qi H, Zhang H, et al. Bacteroides acidifaciens in the gut plays a protective role against CD95-mediated liver injury. Gut Microbes. 2022;14 (1):2027853. doi: 10.1080/19490976.2022.2027853.
20. Shen H, Zhou L, Zhang H, Yang Y, Jiang L, Wu D, Shu H, Zhang H, Xie L, Zhou K, et al. Dietary fiber alleviates alcoholic liver injury via Bacteroides acidifaciens and subsequent ammonia detoxification. Cell Host Microbe. 2024;32(8):1331–1346.e6. doi: 10.1016/j.chom.2024.06.008.
21. Sun L, Xie C, Wang G, Wu Y, Wu Q, Wang X, Liu J, Deng Y, Xia J, Chen B, et al. Gut microbiota and intestinal FXR mediate the clinical benefits of metformin. Nat Med. 2018;24(12):1919–1929. doi: 10.1038/s41591-018-0222-4.
22. Chiang JY. Bile acid metabolism and signaling. Compr Physiol. 2013;3:1191–1212.
23. Hollman DA, Milona A, van Erpecum KJ, van Mil SW. Anti-inflammatory and metabolic actions of FXR: insights into molecular mechanisms. Biochim Biophys Acta. 2012;1821(11):1443–1452. doi: 10.1016/j.bbalip.2012.07.004.
24. Renga B, Mencarelli A, Migliorati M, Cipriani S, D'Amore C, Distrutti E, et al. Shp-dependent and -independent induction of peroxisome proliferator-activated receptor-γ by the bile acid sensor farnesoid X receptor counter-regulates the pro-inflammatory phenotype of liver myofibroblasts. Inflamm Res. 2011;60(6):577–587. doi: 10.1007/s00011-010-0306-1.
25. Feng S, Reuss L, Wang Y. Potential of natural products in the inhibition of adipogenesis through regulation of PPARγ expression and/or its transcriptional activity. Molecules. 2016;21(10):1278. doi: 10.3390/molecules21101278.
26. Singh VK, Seed TM. Radiation countermeasures for hematopoietic acute radiation syndrome: growth factors, cytokines and beyond. Int J Radiat Biol. 2021;97 (11):1526–1547. doi: 10.1080/09553002.2021.1969054.
27. Duhrsen U, Metcalf D. Effects of irradiation of recipient mice on the behavior and leukemogenic potential of factor-dependent hematopoietic cell lines. Blood. 1990;75(1):190–197. doi: 10.1182/blood.V75.1.190.190.
28. Jian Y, Zhang D, Liu M, Wang Y, Xu ZX. The impact of gut microbiota on radiation-induced enteritis. Front Cell Infect Microbiol. 2021;11:586392. doi: 10.3389/fcimb.2021.586392.
29. Maan K, Tyagi R, Dutta A, Bakhshi R, Rana P. Comparative metabolic profiles of total and partial body radiation exposure in mice using an untargeted

metabolomics approach. Metabolomics. 2020;16 (12):124. doi: 10.1007/s11306-020-01742-7.
30. Scanff P, Grison S, Marais T, Gourmelon P, Griffiths NM. Dose dependence effects of ionizing radiation on bile acid metabolism in the rat. Int J Radiat Biol. 2002;78(1):41–47. doi: 10.1080/09553000110087362.
31. Guo H, Chou WC, Lai Y, Liang K, Tam JW, Brickey WJ, Chen L, Montgomery ND, Li X, Bohannon LM, et al. Multi-omics analyses of radiation survivors identify radioprotective microbes and metabolites. Science. 2020;370(6516):370. doi: 10.1126/science.aay9097.
32. Zhang L, Miao Z, Li Y, Xu X, Zhou T, Zhang Y, Liu Y. A potential marker of radiation based on 16S rDNA in the rat model: intestinal flora. PLOS ONE. 2023;18(8): e0286026. doi: 10.1371/journal.pone.0286026.
33. Liu J, Cheng J, Huang M, Shen C, Xu K, Xiao Y, Pan W, Fang Z. Identification of an invertase with high specific activity for Raffinose Hydrolysis and its application in soymilk treatment. Front Microbiol. 2021;12:646801. doi: 10.3389/fmicb.2021.646801.
34. Xu G, Xing W, Li T, Ma Z, Liu C, Jiang N, Luo L. Effects of dietary raffinose on growth, non-specific immunity, intestinal morphology and microbiome of juvenile hybrid sturgeon (Acipenser baeri Brandt ♀ × A. schrenckii Brandt ♂). Fish Shellfish Immunol. 2018;72:237–246. doi: 10.1016/j.fsi.2017.11.001.
35. Collins SL, McMillan A, Seney S, van der Veer C, Kort R, Sumarah MW, Reid G. Promising prebiotic candidate established by evaluation of lactitol, Lactulose, Raffinose, and oligofructose for maintenance of a Lactobacillus-dominated vaginal microbiota. Appl Environ Microbiol. 2018;84(5):84. doi: 10.1128/AEM.02200-17.
36. Then CK, Paillas S, Wang X, Hampson A, Kiltie AE. Association of bacteroides acidifaciens relative abundance with high-fibre diet-associated radiosensitisation. BMC Biol. 2020;18(1):102. doi: 10.1186/s12915-020-00836-x.
37. Pacifici S, Song J, Zhang C, Wang Q, Glahn RP, Kolba N, Tako E. Intra amniotic administration of raffinose and stachyose affects the intestinal brush border functionality and alters gut microflora populations. Nutrients. 2017;9(3):304. doi: 10.3390/nu9030304.
38. Yang JY, Lee YS, Kim Y, Lee SH, Ryu S, Fukuda S, Hase K, Yang C-S, Lim HS, Kim M-S, et al. Gut commensal bacteroides acidifaciens prevents obesity and improves insulin sensitivity in mice. Mucosal Immunol. 2017;10(1):104–116. doi: 10.1038/mi.2016.42.
39. Jia W, Wei M, Rajani C, Zheng X. Targeting the alternative bile acid synthetic pathway for metabolic diseases. Protein Cell. 2021;12(5):411–425. doi: 10.1007/s13238-020-00804-9.
40. Ye X, Huang D, Dong Z, Wang X, Ning M, Xia J, Shen S, Wu S, Shi Y, Wang J, et al. FXR signaling-mediated bile acid metabolism is critical for alleviation of cholesterol gallstones by Lactobacillus strains. Microbiol Spectr. 2022;10(5):e0051822. doi: 10.1128/spectrum.00518-22.
41. Xie Z, Jiang H, Liu W, Zhang X, Chen D, Sun S, Zhou C, Liu J, Bao S, Wang X, et al. The triterpenoid sapogenin (2α-OH-Protopanoxadiol) ameliorates metabolic syndrome via the intestinal FXR/GLP-1 axis through gut microbiota remodelling. Cell Death Dis. 2020;11(9):770. doi: 10.1038/s41419-020-02974-0.
42. Li T, Ding N, Guo H, Hua R, Lin Z, Tian H, Yu Y, Fan D, Yuan Z, Gonzalez FJ, et al. A gut microbiota-bile acid axis promotes intestinal homeostasis upon aspirin-mediated damage. Cell Host & Microbe. 2024;32(2):191–208.e9. doi: 10.1016/j.chom.2023.12.015 .
43. Freire PR, Conneely OM. NR4A1 and NR4A3 restrict HSC proliferation via reciprocal regulation of C/EBPα and inflammatory signaling. Blood. 2018;131 (10):1081–1093. doi: 10.1182/blood-2017-07-795757.
44. Vavassori P, Mencarelli A, Renga B, Distrutti E, Fiorucci S. The bile acid receptor FXR is a modulator of intestinal innate immunity. J Immunol. 2009;183 (10):6251–6261. doi: 10.4049/jimmunol.0803978.
45. Wang YD, Chen WD, Wang M, Yu D, Forman BM, Huang W. Farnesoid X receptor antagonizes nuclear factor κB in hepatic inflammatory response. Hepatology. 2008;48 (5):1632–1643. doi: 10.1002/hep.22519.
46. Chen L, Jiao T, Liu W, Luo Y, Wang J, Guo X, Tong X, Lin Z, Sun C, Wang K, et al. Hepatic cytochrome P450 8B1 and cholic acid potentiate intestinal epithelial injury in colitis by suppressing intestinal stem cell renewal. Cell STEM Cell. 2022;29(9):1366–81 e9. doi: 10.1016/j.stem.2022.08.008.
47. Sigurdsson V, Takei H, Soboleva S, Radulovic V, Galeev R, Siva K, Leeb-Lundberg LM, Iida T, Nittono H, Miharada K. Bile acids protect expanding hematopoietic stem cells from unfolded protein stress in fetal liver. Cell STEM Cell. 2016;18(4):522–532. doi: 10.1016/j.stem.2016.01.002.
48. Feng Y, Yuan P, Guo H, Gu L, Yang Z, Wang J, Zhu W, Zhang Q, Cao J, Wang L, et al. METTL3 mediates epithelial–mesenchymal transition by modulating FOXO1 mRNA N 6 -methyladenosine-dependent YTHDF2 binding: a novel mechanism of radiation-induced lung injury. Adv Sci. 2023;10(17):e2204784. doi: 10.1002/advs.202204784.
49. Wang R, Wu D, Dai J, Shen J, Rong J, Chen Z, Jiao Y, Qi X. USP11 plays a critical role in the onset and progression of acute graft-versus-host disease: novel target for precision therapeutics. Pharmacol Res. 2023;189:106707. doi: 10.1016/j.phrs.2023.106707.
50. Nishi Y, Murakami A, Murayama Y, Tsukahara N, Okamoto S, Nakachi S, Morichika K, Tamaki K, Noguchi H, Matsushita M, et al. Adipose tissue-derived mesenchymal stem cells ameliorate bone marrow aplasia related with graft-versus-host disease in experimental murine models. Transpl Immunol. 2019;55:101205. doi: 10.1016/j.trim.2019.03.004.

51. Chen S, Zhou Y, Chen Y, Gu J. Fastp: an ultra-fast all-in-one FASTQ preprocessor. Bio informatics. 2018;34(17):i884–i90. doi: 10.1093/bioinformatics/bty560.
52. Callahan BJ, McMurdie PJ, Rosen MJ, Han AW, Johnson AJ, Holmes SP. DADA2: High-resolution sample inference from Illumina amplicon data. Nat Methods. 2016;13(7):581–583. doi: 10.1038/nmeth.3869.
53. Bolyen E, Rideout JR, Dillon MR, Bokulich NA, Abnet CC, Al-Ghalith GA, Alexander H, Alm EJ, Arumugam M, Asnicar F, et al. Reproducible, interactive, scalable and extensible microbiome data science using QIIME 2. Nat Biotechnol. 2019;37(8):852–857. doi: 10.1038/s41587-019-0209-9.
54. Douglas GM, Maffei VJ, Zaneveld JR, Yurgel SN, Brown JR, Taylor CM, Huttenhower C, Langille MGI. PICRUSt2 for prediction of metagenome functions. Nat Biotechnol. 2020;38(6):685–688. doi: 10.1038/s41587-020-0548-6.
55. Yang C, Mai J, Cao X, Burberry A, Cominelli F, Zhang L, Elofsson A. ggpicrust2: an R package for PICRUSt2 predicted functional profile analysis and visualization. Bio informatics. 2023;39(8):39. doi: 10.1093/bioinformatics/btad470.
56. Segata N, Izard J, Waldron L, Gevers D, Miropolsky L, Garrett WS, Huttenhower C. Metagenomic biomarker discovery and explanation. Genome Biol. 2011;12(6):R60. doi: 10.1186/gb-2011-12-6-r60.
57. Gu J, Jiao Z, Wang T, Zhang B, Zhao H. Glucans with different degrees of polymerization from Leuconostoc mesenteroides CICC6055: analysis of physicochemical properties and intestinal prebiotic function. IJMS. 2023;25(1):258. doi: 10.3390/ijms25010258.
58. Yang Y, Liu S, Wang P, Ouyang J, Zhou N, Zhang Y, Huang S, Jia Z, Zhang A. DNA-dependent protein kinase catalytic subunit (DNA-PKcs) drives chronic kidney disease progression in male mice. Nat Commun. 2023;14(1):1334. doi: 10.1038/s41467-023-37043-5.